Self-consistent transport dynamics for localized waves

O. I. Lobkis and R. L. Weaver*
Department of Theoretical and Applied Mechanics, University of Illinois, Urbana, Illinois 61801, USA
(Received 24 June 2004; published 21 January 2005)

We find that the Vollhardt and Wolfle self-consistent theory of Anderson localization makes simple predictions for transport dynamics in unbounded one- and two-dimensional media. These predictions are derived and explored and compared with direct numerical simulations.

DOI: 10.1103/PhysRevE.71.011112 PACS number(s): 05.60.Gg, 46.65.+g, 43.20.+g, 42.25.−p

I. INTRODUCTION

While the steady-state intensity of waves in the Anderson-localized regime has been studied extensively for many years [1–3], there has been relatively little attention paid to its dynamics. At moderate distances x from a steady-state source in an unbounded medium, with x comparable to or larger than a localization length ξ, standard theory predicts a steady-state diffuse profile of the mean-square wave amplitude ("energy") that varies as $\exp(-x/\xi)$. This exponential dependence is the prime signature of localization. At large distances from a source, transport is effectively zero. Hence follows the conclusion, valid in the thermodynamic limit, that diffusion is zero in localizing systems and the understanding that the Anderson localization of single-electron wave functions is a critical part of the metal-insulator transition in disordered conductors [2].

Classical wave systems [4,5] are understood to localize as well; there is no essential difference between the wave equation for noninteracting electrons and that for electromagnetic or acoustic waves. The most significant differences are practical. One such is due to absorption: observation of an exponential steady state $\exp(-x/L)$ does not permit the identification $L=\xi$. Many measurements are restricted to boundaries; x dependence is not available for study. In classical wave systems the prime signature of localization is probably more clear in transport dynamics than it is in steady-state transmission [5].

Theory for the dynamics of wave energy transport in localizing systems is relatively undeveloped, numerical simulations [6–11] not withstanding. It is widely presumed that, for sufficiently early times and short distances (e.g., Ref. [12]), transport away from an impulsive plane source can be approximated by classical diffusion with a Boltzmann diffusivity D_0: $E \sim \exp(-x^2/4D_0t)/\sqrt{4\pi D_0 t}$. The manner in which this spreading Gaussian evolves at late time into $E \sim \exp(-x/\xi)$ is unclear. Recently Cheung *et al.* [13] and Skipetrov and van Tiggelen [14] have applied the self-consistent theory of Anderson localization [15] to the problem of predicting transport dynamics in quasi-one-dimensional semi-infinite structures. Here we report an application of the same theory to unbounded systems, for which the equations simplify. We find a closed-form expression describing the transport in one-dimensional (1D) systems and simple integral expressions for transport in 2D systems and in an unbounded strip with periodic boundary conditions. Closed-form asymptotic approximations for these latter cases are found to be accurate. The results are compared to those of numerical simulations in the literature.

We consider the self-consistent theory of Anderson localization from [14,15], where the diffusivity $D(\Omega)$ has a dependence on (outer) frequency Ω. Thus the Fourier transform of the response C to an impulsive addition of wave energy at the origin is given by the solution to

$$[-D(\Omega)\nabla^2 + i\Omega]C(\Omega,D,\mathbf{r}) = \delta(\mathbf{r}). \quad (1)$$

The dynamic diffusivity $D(\Omega)$ is given as the solution of

$$\frac{1}{D(\Omega)} = \frac{1}{D_0} + \frac{2}{\alpha}C(\Omega,D,\mathbf{r}=\mathbf{0}), \quad (2)$$

where D_0 is the Boltzmann diffusivity, the effective diffusion constant on a bare microphysical length scale comparable to the mean free path. The parameter α is related to the modal density. Equations (1) and (2) are coupled. Equation (2) describes how the diffusivity is renormalized by the backscattered intensity $C(\mathbf{r}=0)$. Implicit in Eq. (2) is the familiar notion that localization is an extrapolation from weak localization. That this is strictly speaking incorrect may be recognized by considering the case of broken time-reversal invariance where there is no weak localization, but modes are localized. Nevertheless, the theory has enjoyed some success.

In the next three sections we present solutions of Eqs. (1) and (2) in three different systems: in unbounded one- and two-dimensional structures and an in infinite strip of width L with periodic lateral boundary conditions that is intermediate between one dimension and two dimensions and has been studied numerically elsewhere. In all cases we then obtain the corresponding prediction for the quasi-1D response $E(x,t)$, the response to an impulsive addition of wave energy at all points $x=0$. $E(x,t)$ is given in terms of an integral that is evaluated numerically. In Sec. V, this integral is found to be accurately approximated at all points $x>\xi$ by an asymptotic expression. We emphasize the parameter regime most relevant to transport in classical wave localized systems, distances of order 1 to several localization lengths, and

*Corresponding author. FAX: 217-244-5707. Electronic address: r-weaver@uiuc.edu

modest time scales. The results are compared with certain features observed in large-scale direct numerical simulations.

II. UNBOUNDED ONE-DIMENSIONAL SYSTEM

For an unbounded 1D system the function $C(r)$ can be calculated by taking the Fourier transform over the wave number q of both sides of Eq. (1). The result is $C(q)=[D(\Omega)q^2+i\Omega]^{-1}$ and the dynamic diffusion coefficient $D(\Omega)$ is expressed from Eq. (2) as

$$\frac{1}{D(\Omega)}=\frac{1}{D_0}+\frac{2}{2\pi\alpha}\int_{-\infty}^{+\infty}\frac{dq}{D(\Omega)q^2+i\Omega}. \tag{3}$$

Without loss of generality we choose length and time units such that $D_0=\alpha=1$. The integral in Eq. (3) can be calculated simply from the pole at $q=\sqrt{-i\Omega/D(\Omega)}$ and we rewrite Eq. (3) as

$$D(\Omega)=1-\sqrt{\frac{D(\Omega)}{i\Omega}}, \tag{4}$$

which has the solution

$$D(\Omega)=1+\frac{1}{2i\Omega}(1-\sqrt{1+4i\Omega})=\frac{\sqrt{1+4i\Omega}-1}{\sqrt{1+4i\Omega}+1}. \tag{5}$$

Dynamic transport $E(x,t)$ is expressed as the inverse temporal and spatial Fourier transforms of the function C in (Ω,q) space $C(\Omega,q)=[D(\Omega)q^2+i\Omega]^{-1}$:

$$E(x,t)=\frac{1}{4\pi^2}\int\exp(i\Omega t)d\Omega\int_{-\infty}^{+\infty}\frac{\exp(iqx)dq}{D(\Omega)q^2+i\Omega}$$
$$=\frac{i}{4\pi}\int\frac{\exp[i\Omega t+ix\sqrt{-i\Omega/D(\Omega)}]}{\sqrt{-iD(\Omega)\Omega}}d\Omega, \tag{6}$$

where the integration path over Ω is located in the lower complex half-plane. We have taken $x>0$ without loss of generality, as $E(x)=E(-x)$. Using the solution (5) for $D(\Omega)$ the integral (6) for energy can be rewritten as

$$E(x,t)=\frac{\exp(-x)}{2\pi}\int_{-\infty-i\delta}^{+\infty-i\delta}\frac{\exp[i\Omega t-x(\sqrt{1+4i\Omega}-1)/2]}{\sqrt{1+4i\Omega}-1}d\Omega, \tag{7}$$

with an arbitrary $\delta>0$. The integrand in Eq. (7) has a simple pole at $\Omega=0$ and a branch point at $\Omega=i/4$. The pole governs the late-time behavior $E(x,t=\infty)=\exp(-x)/2$. The integral (7) can be calculated analytically in the following manner. Writing $E(x,t)=\exp(-x)I(x,t)/2\pi$, we find

$$\frac{\partial I}{\partial x}=-\frac{\exp(x/2)}{2}\int_{-\infty-i\delta}^{+\infty-i\delta}\exp\left(i\Omega t-\frac{x}{2}\sqrt{1+4i\Omega}\right)d\Omega. \tag{8}$$

The pole at $\Omega=0$ has been eliminated. We deform the integration path from the lower to upper complex half-plane until $\Omega=i/4$. After the substitution $\Omega\to\Omega+i/4$ and transformation of the integration path only over positive real Ω we rewrite it as

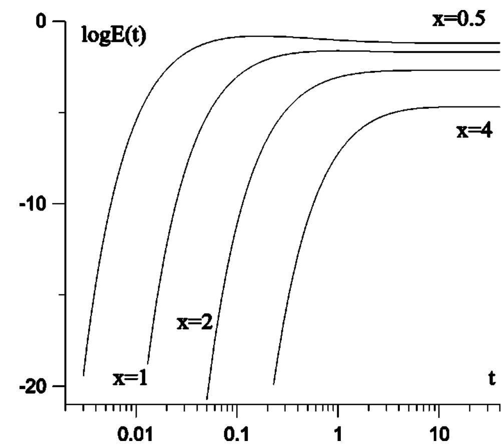

FIG. 1. The solution (12) to the dynamic self-consistent transport equations in 1D, expressed as a function of dimensionless time and for several distances x from the source. Length units are such that localization length $\xi=1$. Time units are such that $D_0=1$. The behavior is similar to that observed in direct numerical simulations [8]. Logarithms, log, are in base e for all figures.

$$\frac{\partial I}{\partial x}=-\exp\left(\frac{x}{2}-\frac{t}{4}\right)\int_0^{\infty}\exp(-x\sqrt{\Omega/2})\cos(\Omega t-x\sqrt{\Omega/2})d\Omega. \tag{9}$$

The substitution $\Omega=2s^2$ simplifies the integral and we find ([16], p. 458)

$$\frac{\partial I}{\partial x}=-4\exp\left(\frac{x}{2}-\frac{t}{4}\right)\int_0^{\infty}\exp(-xs)\cos(2ts^2-xs)s\,ds$$
$$=-\frac{x}{2}\sqrt{\frac{\pi}{t^3}}\exp\left(\frac{x}{2}-\frac{t}{4}-\frac{x^2}{4t}\right). \tag{10}$$

The energy distribution $E(x,t)$ can be expressed by means of $\partial I/\partial x$ as

$$E(x,t)=-\frac{\exp(-x)}{2\pi}\int_x^{\infty}\frac{\partial I}{\partial x}dx$$
$$=\frac{\exp(-x)}{4\sqrt{\pi t^3}}\int_x^{\infty}\exp\left(\frac{x}{2}-\frac{t}{4}-\frac{x^2}{4t}\right)x\,dx. \tag{11}$$

The last integral is represented in terms of the complementary error function erfc, and finally we obtain

$$E(x,t)=\frac{1}{2}\exp(-x)\left(\frac{\exp(-y^2)}{\sqrt{\pi t}}+1-\frac{1}{2}\mathrm{erfc}(y)\right)$$
$$=\left(\frac{\exp\left(-\frac{(x+t)^2}{4t}\right)}{2\sqrt{\pi t}}+\frac{1}{4}\exp(-x)\mathrm{erfc}(-y)\right), \tag{12}$$

where $y=\sqrt{t}/2-x/(2\sqrt{t})$. Plots of $E(x)$ and $E(t)$ are presented in Figs. 1 and 2 for different t and x.

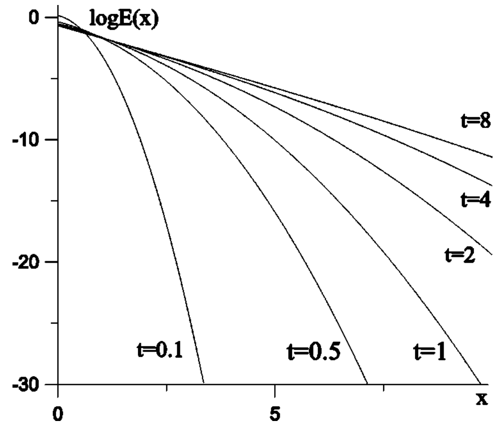

FIG. 2. As in Fig. 1, but expressed as a function of distance for several times. The profile may be observed to approach $\exp(-x)/2$ at late time.

The expressions simplify in the asymptotic limits. For a late time $t \gg x$ the argument y is large and positive and we expand the complementary error function as $\text{erfc}(y) \approx \exp(-y^2)/\sqrt{\pi}y$:

$$E(t \gg x) \approx \frac{1}{2}\exp(-x)\left(1 + \frac{\exp(-y^2)}{\sqrt{\pi t}}\frac{x}{t}\right). \qquad (13)$$

For $t \to \infty$ we recover the expected distribution of energy in localized media $E(x) \approx \frac{1}{2}\exp(-x)$ with unit localization length. For the opposite limit of a distant point at short time $x \gg t$, y is large and negative, and the complementary error function $\text{erfc}(y) = 2 - \text{erfc}(|y|) \approx 2 - \exp(-y^2)/\sqrt{\pi}|y|$. In classical wave systems with realistic levels of absorption, this limit may be most accessible. After cancellation of like terms in Eq. (12) the energy distribution E is found to be

$$E(x \gg t) \approx \exp\left(-\frac{(x+t)^2}{4t}\right)\frac{1+t/x}{2\sqrt{\pi t}}$$

$$= \exp\left(-\frac{x}{2} - \frac{t}{4} - \frac{x^2}{4t}\right)\frac{1+t/x}{2\sqrt{\pi t}}. \qquad (14)$$

At early times, but large distances, the behavior is not classical diffusion $\exp(-x^2/4t)/\sqrt{4\pi t}$, but is diminished by a factor $\exp(-x/2 - t/4)$; this is the earliest sign of localization to manifest at large distances. It may be noted that the behavior is not representable in terms of a time-dependent diffusivity, but is equivalent to classical diffusion under an envelope $\exp(-x/2)$ with an effective localization length twice the actual length and an augmented absorptivity $\exp(-t/4)$.

III. UNBOUNDED TWO-DIMENSIONAL SYSTEM

The solution of Eq. (2) for the dynamic diffusion coefficient $D(\Omega)$ in 2D can be presented in the same manner as for 1D case:

$$\frac{1}{D(\Omega)} = \frac{1}{D_0} + \frac{2}{(2\pi)^2\alpha}\int_0^{q_{\max}} \frac{2\pi q\, dq}{D(\Omega)q^2 + i\Omega}, \qquad (15)$$

where $q_{\max}$ is a cutoff wave number related to a microscopic length l_{mic} as $q_{\max} = 1/l_{mic}$ upon which a Boltzmann diffusivity D_0 may be described. We obtain an implicit form for the connection between D and Ω,

$$\Omega = \frac{iD\Phi}{1 - \exp[\beta(1 - D/D_0)]}, \qquad (16)$$

where the quantities $\beta = 2\pi\alpha$ and $\Phi = q_{\max}^2$ have been introduced. In the stationary regime $(\Omega \to 0)$ the diffusion coefficient $D \approx i\xi^2\Omega$, where ξ is the localization length. Comparing this with Eq. (16) we find $\xi = \{[\exp(\beta) - 1]/\Phi\}^{1/2}$. A regime of universal behavior independent of the details of the microscale is presumably obtained in the limit $\xi \gg l_{mic}$—i.e., $\exp(\beta) \gg 1$ and $\xi \approx [\exp(\beta)/\Phi]^{1/2}$. It is in this regime that we focus further attention. The function $D(\Omega)$ has two branch points. They are on the positive imaginary Ω axis and are the solutions of the equation $\Omega'(D) = 0$. $\Omega_{1,2} = iD_0\Phi u_{1,2}/\beta$ where $u_1 < 1$ and $u_2 > 1$ are two solutions of the simple equation $u\exp(-u) = \exp(-\beta - 1)$. For the universal regime $\exp(\beta) \gg 1$ the branch points simplify: $\Omega_1 \approx iD_0/e\xi^2\beta$ and $\Omega_2 \approx iD_0\Phi$ where $e = 2.718\ldots$. The branch point Ω_2 is unimportant except on the microscale and will be ignored. We rewrite Ω_1 as $\Omega_1 \approx i/4\tau$ where $\tau = e\xi^2\beta/4D_0$ is a characteristic time of transport. In all further numerical calculations we will choose length and time units such that $\xi = 1$ and $\tau = 1$, thus permitting comparison with the one-dimensional case without further loss of generality.

Once again the energy distribution $E(\mathbf{r}, t)$ is expressed as the inverse temporal and spatial Fourier transforms of the function $C(\Omega, q)$ as

$$E(\mathbf{r}, t) = \frac{1}{(2\pi)^3}\int \exp(i\Omega t)d\Omega \int \frac{f(\mathbf{q})\exp(i\mathbf{q}\cdot\mathbf{r})d^2q}{D(\Omega)q^2 + i\Omega}, \qquad (17)$$

where $f(\mathbf{q})$ is the source function. For a point source at the origin $f(\mathbf{q}) = 1$, and for a line source located along the y axis $f(\mathbf{q}) = 2\pi\delta(q_y)$. Here we will consider further only a line source. After calculation of the integral over q_y and q_x we write

$$E(x, t) = \frac{i}{4\pi}\int_{-\infty - i\delta}^{+\infty - i\delta} \frac{\exp[i\Omega t + ix\sqrt{-i\Omega/D(\Omega)}]}{\sqrt{-iD(\Omega)\Omega}}d\Omega, \qquad (18)$$

as in Eq. (6), except that the diffusion coefficient is now determined by Eq. (16), not Eq. (5). The integral (18) can be calculated numerically. As expected, when space and time units are chosen as before such that $\xi = 1$ and the branch point is at $i/4$, and in the limit $\exp(\beta) \gg 1$, the behavior is independent of the microphysics β, Φ, and D_0. The resulting temporal and spatial distributions are presented in Figs. 3 and 4. For comparison with the 1D case, selected curves from Figs. 1 and 2 are overlaid. In units such that the behavior at late time is identical $(\xi = 1, \tau = 1)$, transport in 2D is substantially faster than it is in 1D.

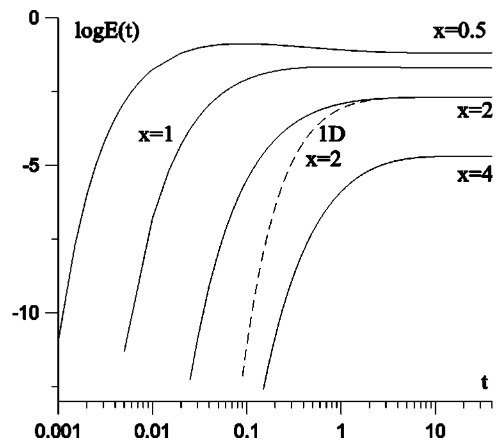

FIG. 3. The solution of the dynamic self-consistent transport equation in 2D as evaluated by numerical integration of integral (18). Length units are such that $\xi=1$; time units are such, as in Figs. 1 and 2, that the branch point $\Omega_{bp}=i/4$—i.e., $\tau=1$. One of the curves from Fig. 1 is overlaid for comparison.

IV. INFINITE STRIP

We consider a strip of infinite length $-\infty < x < \infty$ but finite width $0 < y < L$. It is a case intermediate between the 1D and 2D cases considered above. Periodic boundary conditions $C(x,y)=C(x,y+L)$ are invoked, consistent with those employed in direct numerical simulations [8,10]. Such boundary conditions assure invariance in the y direction and no y dependence in $D(\Omega)$. The solution of Eq. (2) is presented as a sum of the solution for an unbounded 2D medium $K_0(x\sqrt{i\Omega/D})$ plus additional terms corresponding to image sources $K_0((i\Omega/D)^{1/2}r_n)$, where K_0 is the modified Bessel function and $r_n=\sqrt{x^2+L^2n^2}(n\neq 0)$ is the distance to the nth image source:

$$C(x) = \frac{1}{2\pi D}K_0\left(x\sqrt{\frac{i\Omega}{D}}\right) + \frac{1}{2\pi D}\sum_{n=-\infty,n\neq 0}^{\infty} K_0\left(\sqrt{(x^2+L^2n^2)\frac{i\Omega}{D}}\right). \quad (19)$$

The first term on right-hand side of Eq. (19), when evaluated

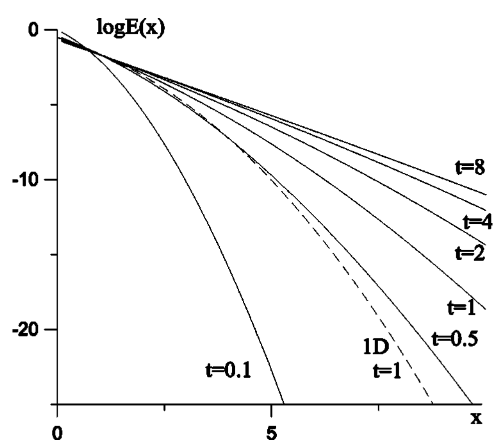

FIG. 4. The integral (18) expressed as a function of distance x at several times.

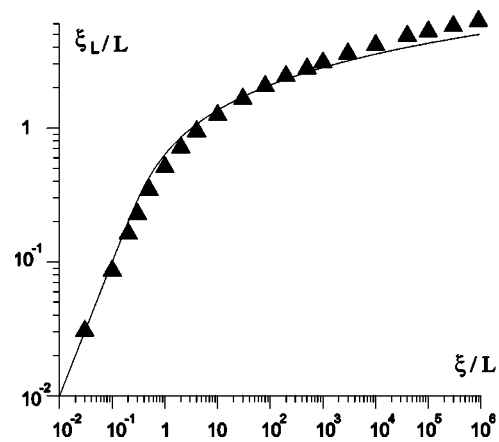

FIG. 5. The localization length ξ_L in a strip of width L is compared with that of an unbounded 2D system with the same microstructure. The solid line is the prediction of the self-consistent theory, Eq. (23). The isolated points are taken from the direct numerical simulations of MacKinnon and Kramer [10].

at $x=0$, of course requires due attention to the length scale cutoff l_{mic}. Equation (2) for the dynamic diffusion coefficient becomes

$$\frac{1}{D(\Omega)} = \frac{1}{D_0} + \frac{2}{(2\pi)^2\alpha}\int_0^{q_{\max}} \frac{2\pi q\, dq}{D(\Omega)q^2 + i\Omega} + \frac{2}{2\pi D\alpha}\sum_{n=-\infty,n\neq 0}^{n=\infty} K_0\left(L|n|\sqrt{\frac{i\Omega}{D}}\right), \quad (20)$$

which can be rewritten in the same form as Eq. (16):

$$\Omega = \frac{iD\Phi}{1-\exp[\beta(1-D/D_0) - 4\sum_{n=1}^{n=\infty} K_0(Ln\sqrt{i\Omega/D})]}. \quad (21)$$

Once again we insist that in the stationary limit $(\Omega\to 0)$ the diffusion coefficient $D\approx i\xi_L^2\Omega$, where ξ_L is the localization length in the strip. As the result we obtain

$$\xi_L^2 = \frac{\exp\left[\beta - 4\sum_{n=1}^{n=\infty} K_0(Ln/\xi_L)\right] - 1}{\Phi}. \quad (22)$$

In the universal regime $\xi \gg l_{mic}$, equivalent to $\exp(\beta)\gg 1$, the localization length $\xi^2\approx \exp(\beta)/\Phi$ and Eq. (22) may be rewritten as a relation between the localization length ξ_L for strip of width L and the localization length ξ for an unbounded 2D medium with the same microphysics D_0, l_{mic}, and β:

$$\xi = \xi_L \exp\left(2\sum_{n=1}^{\infty} K_0(Ln/\xi_L)\right). \quad (23)$$

A graph of ξ_L/L versus ξ/L from Eq. (23) is drawn in Fig. 5 as a solid line. For comparison, the results of numerical simulations of MacKinnon and Kramer [10] are presented in the same graph as symbols. The similarity of the curves is

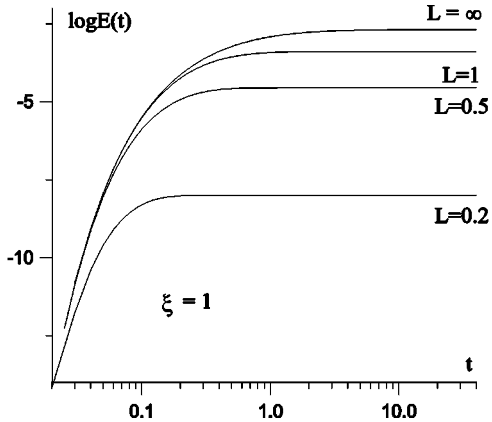

FIG. 6. Comparison of transport dynamics at $x=2$ in strips of various widths L. Microstructural parameters are identical to those of Figs. 3 and 4.

encouraging. The slight differences are not explained, but are presumably due to failure of the self-consistent (SC) model.

The transport dynamics of a strip is described by Eq. (18) with the dynamic diffusion coefficient from Eq. (21). Figure 6 presents the $E(t)$ dependence at distance $x/\xi=2$, and Fig. 7 presents the $E(x)$ dependence at time $t=1$ for different L. Again we have chosen $\tau = e\xi^2\beta/4D_0 = 1$ so that the transport rates in Figs. 3 and 6 may be compared. A comparison of Fig. 6 and the $x/\xi=2$ curve of Fig. 3 shows that the transition to stationary conditions takes place more rapidly in the strip. For the same microphysics, the strip has a shorter localization length and the transport time ξ_L^2/D_0 is shorter than ξ^2/D_0.

V. ASYMPTOTICS: COMPARISON OF THE DYNAMICS FOR 1D AND 2D AND STRIP

The numerical integral (18) can be evaluated asymptotically, thus facilitating understanding and better allowing comparison between the transport dynamics in the different structures. All transport is governed by the same integral (18), the only difference being the different $D(\Omega)$, expressed by Eqs. (5), (16), and (21), respectively. To estimate the integral we make the substitution $i\Omega/D(\Omega)=p^2$ and rewrite Eq. (18) as

$$E(x,t) = \frac{i}{4\pi}\int_{C_p} \exp[S(p)]\frac{\Omega'(p)}{ipD(p)}dp$$
$$= -\frac{i}{2\pi}\int_{C_p} \exp[S(p)]dp - \frac{i}{4\pi}\int_{C_p} \exp[S(p)]f(p)dp, \tag{24}$$

where the exponent $S(p)=i\Omega(p)t - xp = tpD(p) - xp$ and the integrand $f(p)=pD'(p)/D(p)$. The three cases differ in their $D(p)$ dependences (given below). The integration contours C_p in the complex p plane are mapped from the original contour in the Ω plane (from $-\infty - i\delta$ to $\infty - i\delta$) and are presented in Fig. 8. The pole p_0 of the function $f(p)$ is located at the vertex of the integration contour on the real p axis. It corresponds to the point $\Omega=0$ and can be calculated as a limit of the ratio $i\Omega/D(\Omega)$ for small Ω, $p_0\sqrt{i\Omega/D(\Omega)}|_{\Omega=0} = 1/\xi$ (or $1/\xi_L$). At large t and/or x the integrals (24) can be evaluated by the saddle-point method. We present the integrand $f(p)$ near the pole p_0 as

$$f(p) = \frac{p_0}{p - p_0} + \sum_{n=0}^{\infty} B_n(p_s,p_0)(p-p_s)^n, \tag{25}$$

where the residue of the function $f(p)=pD'(p)/D(p)$ at the pole p_0 is equal to p_0 and the second term here is the regular part of the function $f(p)$ expanded around p_s. The saddle point p_s is a solution of the equation $S'(p_s)=0$. The coefficients $B_n(p_s,p_0)$ can be determined by standard procedures. After substitution of Eq. (25) into Eq. (24) and regrouping of the terms we rewrite it as

$$E(x,t) = -\frac{i}{4\pi}\int_{C_p} \exp[S(p)]\left(2 + \sum_{n=0}^{\infty} B_n(p_s,p_0)(p-p_s)^n\right)dp$$
$$-\frac{ip_0}{4\pi}\int_{C_p} \exp[S(p)]\frac{dp}{p-p_0}. \tag{26}$$

Thus the transport dynamics is presented as a sum of two

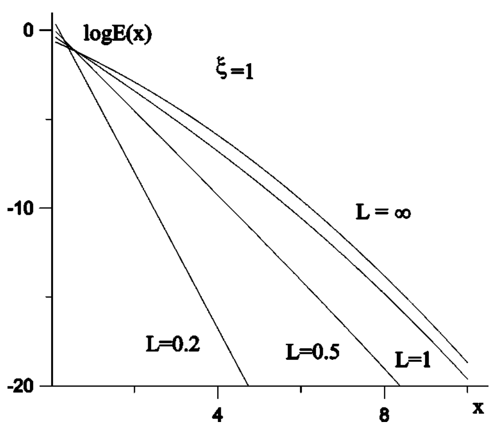

FIG. 7. Comparison of transport dynamics at $t=1$ in strips of various widths L.

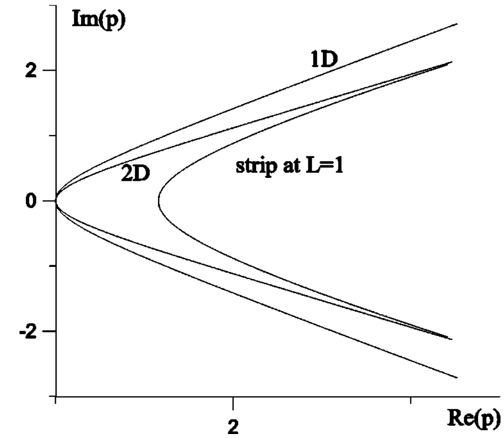

FIG. 8. The integration contours C_p are mapped from the original contours in the Ω plane $(-\infty - i\delta, \infty - i\delta)$.

terms. The first does not include any contribution from the pole and dominates the dynamics for short times. We will call it the diffusionlike term. The second term includes a contribution from the pole and is dominant for late times. We will call it the localizationlike term. Calculation of both using the residue theorem and the saddle-point method is straightforward; the solution is

$$E(x,t) \approx \sqrt{\frac{1}{2\pi S''(p_s)}}\left(1+\frac{1}{2}B_0(p_s,p_0)\right)\exp[S(p_s)] + \frac{p_0\exp(-p_0x)}{4}\text{erfc}[\sqrt{S''(p_s)/2}(p_s-p_0)], \quad (27)$$

where $S''(p_s)$ is the second derivative of the exponent S at the saddle point and the coefficient $B_0(p_s,p_0)$ is equal to $f(p_s) - p_0/(p_s-p_0)$.

The simplest form of the functions $D(p)$ and $S(p)$ is obtained in the 1D case, where $D_1(p)=1-1/p$, the corresponding exponent is $S_1(p)=tp(p-1)-xp$, and the integrand is $f_1(p)=1/(p-1)$. Calculating the first derivative of the function $S_1(p)$ we find that the saddle point for 1D is at $p_{s1} = (x+t)/2t$. This is located on the real p axis. Similarly, $S_1(p_{s1})=-(x+t)^2/4t$ and $S_1''(p_{s1})=2t$. The asymptotic expression (27) is found to equal the exact solution (12). Because of the simple form of the integrand $f_1(p)$ and because the exponent $S_1(p)$ is a quadratic, the asymptotic expression is exact.

The diffusion coefficient $D_2(p)$ for the unbounded 2D case can be presented in explicit form as

$$D_2(p) = \frac{D_0}{\beta}\left[\beta - \ln\left(\frac{\Phi}{p^2}+1\right)\right]. \quad (28)$$

In the universal regime $\exp(\beta) \gg 1$, at both points p of interest, and for all realistic values of x and t, the ratio Φ/p^2 is large. The pole p_0 is at $1/\xi$ and $\Phi/p_0^2=(\xi/l_{mic})^2 \gg 1$. The saddle point is such that $\Phi/p_s^2 \sim (\xi/l_{mic})^2(\xi t/x\tau)^2 \gg 1$ except at very large x/t. This allows Eq. (28) to be simplified,

$$D_2(p) \approx \frac{2D_0}{\beta}\ln(p\xi) = \frac{e\xi^2}{2\tau}\ln(p\xi), \quad (29)$$

now expressed in terms of macroscopic parameters. The exponent for the 2D case is $S_2(p) \approx e\xi^2 tp^2 \ln(p\xi)/2\tau - xp$ and the corresponding equation for the saddle point p_{s2} is

$$p_{s2}[2\ln(p_{s2}\xi)+1] - b = 0, \quad (30)$$

where $b=2x\tau/e\xi^2 t$. The exponent at the saddle point is $S_2(p_{s2}) \approx -e\xi^2 tp_{s2}^2/4\tau - xp_{s2}/2$ and its second derivative $S_2''(p_{s2})=e\xi^2 t[3+2\ln(p_{s2}\xi)]/2\tau$. The coefficients $B_0(p_{s2} \neq \xi^{-1})=\ln^{-1}(p_{s2}\xi)-(p_{s2}\xi-1)^{-1}$ and $B_0(p_{s2}=\xi^{-1})=1/2$. Graphs of $E(x)$ for 2D unbounded media are presented in Fig. 9 for different t where the exact solutions of integral (18) are solid lines and the asymptotic solutions (27) are dashed lines. Except at short x, the asymptotic expression is highly accurate. Figure 10 presents $E(t)$ for $x/\xi=1$ and $x/\xi = 2$. The maximum relative difference between exact and approximate curves occurs at smaller distances and is 10%–20%. For 2D unbounded media the approximation (27) describes the transport dynamics well for all distances greater than the localization length ξ.

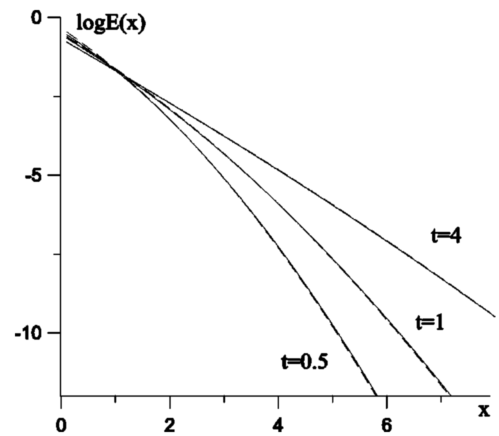

FIG. 9. Comparison of the exact (solid lines) and asymptotic (dashed lines) spatial dependence of transport dynamics in 2D.

The diffusion coefficient $D_L(p)$ for a strip can be also presented in explicit form in the complex p plane:

$$D_L(p) = \frac{D_0}{\beta}\left[\beta - \ln\left(\frac{\Phi}{p^2}+1\right) - 4\sum_{n=1}^{\infty}K_0(Lnp)\right] \approx \frac{e\xi^2}{2\tau}\left(\ln(p\xi) - 2\sum_{n=1}^{\infty}K_0(Lnp)\right). \quad (31)$$

The structure of the exponent function S_L for a strip can be considered in the same manner as for the 2D case and we find $S_L(p)=e\xi^2 tp^2[\ln(p\xi)-2\Sigma_{n=1}^{\infty}K_0(Lnp)]/2\tau - xp$. The saddle point in the limit $\Phi/p_{sL}^2 \gg 1$ is the solution of

$$p_{sL}\left(2\ln(p_{sL}\xi)+1-4\sum_{n=1}^{\infty}K_0(Lnp_{sL})+2\sum_{n=1}^{\infty}Lnp_{sL}K_1(Lnp_{sL})\right) - b = 0, \quad (32)$$

and the transport dynamics can be easy calculated for a strip of arbitrary width L using Eqs. (27), (31), and (32).

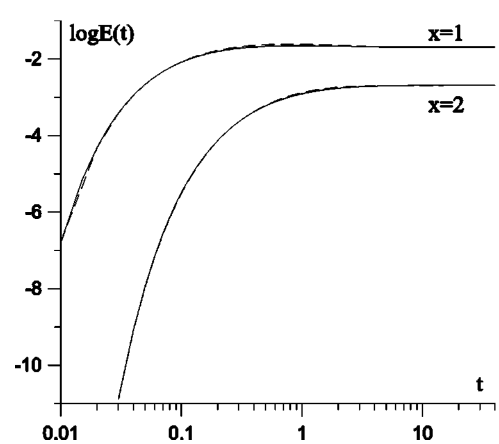

FIG. 10. Comparison of the exact (solid lines) and asymptotic (dashed lines) temporal dependence of transport dynamics in 2D.

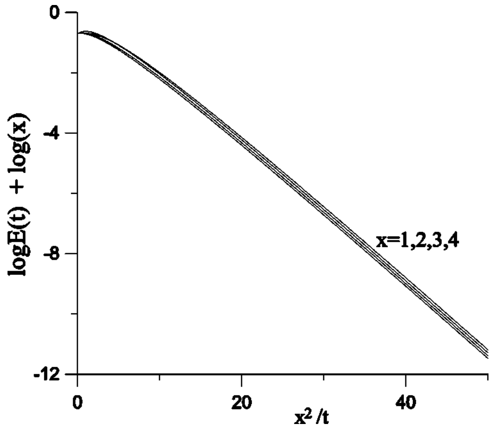

FIG. 11. The predictions for transport dynamics in 1D are plotted versus x^2/t. A phenomenological form $\exp(-x-x^2/4D_{eff}t)$ approximately fits the data.

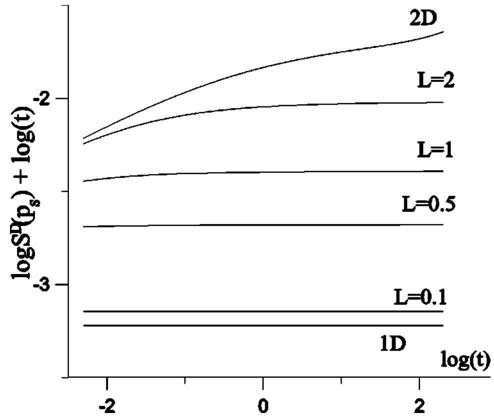

FIG. 13. The slope of the exponent $S^D(p_s)$ versus $\log t$ for 1D and 2D and strips of different widths L is close to -1, except in 2D where it varies but has a value near -0.8.

VI. COMPARISON WITH NUMERICAL SIMULATION OF TRANSPORT

Direct numerical simulations [7,8] have emphasized a striking apparent collapse of transport data to a phenomenological form $\exp(-x/\xi)\exp[-(x^{n+2}/4D_{eff}\xi^n t)^\gamma]$ over a substantial dynamic range for all $x>2\xi$ and $t<x$. In 1D Weaver and Burkhardt [8] studied a strip with periodic lateral boundary conditions in the parametric regime mean free path $\ll$ width $\ll$ localization length. The system was thus quasi 1D. They found $n=0$ and $\gamma=1$. In 2D Weaver [7] studied the same sort of structure, but in the limit mean free path $\ll$ localization length $\ll$ width. The system was thus 2D. He found $n\approx 0.46$ and $\gamma\approx 0.76$. This precise form is not confirmed by the current calculations. Nevertheless, when the exact or asymptotic expressions are plotted in Figs. 11 and 12 in the manner suggested by [7,8] we see that these forms are well supported by the present theory for all $x>2\xi$ and $E>e^{-10}$. Thus the SC theory of transit dynamics is consistent with these direct numerical simulations.

In an attempt to find a theoretical basis for these exponents we note that the main features of transport at $x>t$ are determined by the x and t dependences of the exponent S at the saddle point p_s in the first term of Eq. (27). In general, the exponent $S(p_s)$ can be presented as the sum of three terms. It contains two terms linear in x and t which describe an additional diminishing of energy because of localization, plus a diffusionlike term $S^D(p_s)\sim -x^{1+\gamma}/t^\gamma$, where the parameter γ depends on the geometry of the problem. For $x>t$ this term is dominant and we can investigate the scaling of the transport of localizing waves based only on the x and t dependences of the function S^D.

For the 1D case where an explicit form of the exponent is possible, $S_1(p_{s1})=-(x+t)^2/4t=-t/4-x/2-x^2/4t$ and $S_1^D(p_{s1})=-x^2/4t$ in accordance with the numerical calculations of Weaver and Burkhardt [8]. For the 2D case the exponent can be presented only in implicit form but linear terms over t and x can be separated and $S_2(p_{s2})=-t/4\tau-x/\xi\sqrt{e}+S_2^D(p_{s2})$. Because of the logarithmic dependence of the saddle point for 2D media, $S^D(p_s)\sim -x^{1+\gamma}/t^\gamma$ cannot be described by constant γ for all x and t. Estimation of the diffusionlike term S_2^D shows that for short distance or late time $x<t$ (i.e., near the stationary regime), scaling is close to that of classical diffusion: $S_2^D(p_{s2})\sim -x^2/t$. For the opposite

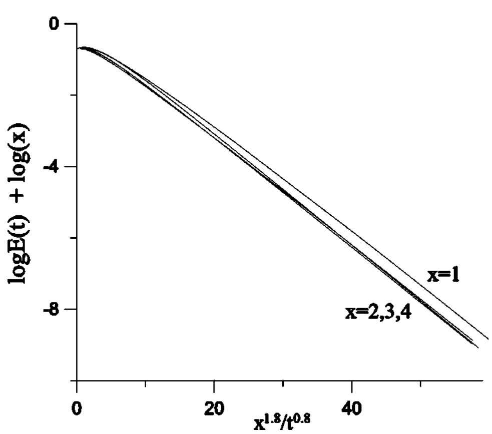

FIG. 12. Transport dynamics in 2D approximately fits the phenomenological form $\exp[-x-(x^{2+n}/D_{eff}\xi^n t)^\gamma]$ with $\gamma=0.8$ and $n=0.25$.

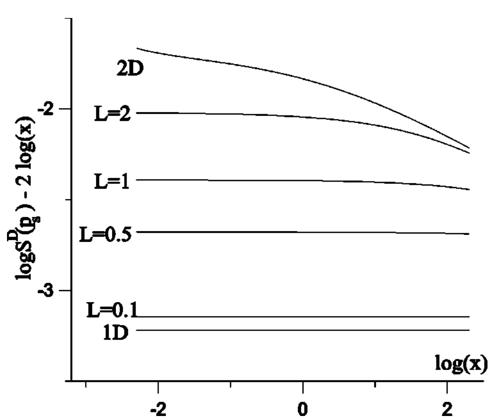

FIG. 14. The slope of the exponent $S^D(p_s)$ versus $\log x$ for 1D and 2D and strips of different widths L is close to +2 except in 2D where it varies but has a value close to 1.8.

limit $x > t$, far from stationary regime and arguably the more relevant for experiments, we have approximately $S_2^D(p_{s2}) \sim -x^{1.8}/t^{0.8}$, close to the phenomenological observations of Weaver [7]. This is illustrated in Figs. 13 and 14. The slopes of the log-log plots are such that a dependence x^2/t is apparent in 1D. The slope in the 2D case varies slowly with x and t, but is close to $x^{1.8}/t^{0.8}$ over a substantial range in x and t.

It is clear that for $L/\xi > 1$ the strip localization length $\xi_L \approx \xi$ and the values of the sums in Eq. (32) are small. As a result, Eq. (32) transforms to Eq. (30) and we find the same dynamics for the strip as for an infinite 2D medium. For the opposite case $L/\xi < 1$ we find the same dependence as in 1D where $p_{sL} \sim \text{const} + x/t$ and $S_L^D(p_{sL}) \sim -x^2/t$. The x and t dependences of the function $S^D(p_s)$ for 1D and 2D and a strip are presented in Figs. 13 and 14.

VII. CONCLUSIONS

Integral expressions for dynamic transport of Anderson localized waves have been derived with the self-consistent theory of localization. In 1D they are evaluated in closed form; in 2D and in a strip geometry, they require numerical or asymptotic evaluation. Early-time behavior is found to differ subtly but significantly from the common presumption of classical diffusion. We find that the theory does a good job of reproducing key features observed in direct numerical simulations.

ACKNOWLEDGMENTS

The authors thank Bart van Tiggelen for useful discussions. This work was partially supported by the National Science Foundation through Grant CMS-0201346.

[1] E. Abrahams, P. W. Anderson, D. C. Licciardello, and T. V. Ramakrishnan, Phys. Rev. Lett. **42**, 673 (1979).
[2] P. A. Lee and T. V. Ramakrishnan, Rev. Mod. Phys. **57**, 287 (1985).
[3] Scattering and Localization of Classical Waves in Random Media, edited by P. Sheng, *World Scientific Series on Directions in Condensed Matter Physics*, Vol. 8 (World Scientific, Singapore, 1990).
[4] A. Z. Genack and A. A. Chabanov, in *Waves and Imaging Through Complex Media*, edited by P. Sebbah (Kluwer, Dordrecht, 2001), pp. 53–84; D. S. Wiersma *et al.*, Nature (London) **390**, 671 (1997).
[5] R. Weaver, Wave Motion **12**, 129 (1990).
[6] R. L. Weaver, Phys. Rev. B **47**, 1077 (1993).
[7] R. L. Weaver, Phys. Rev. B **49**, 5881 (1994).
[8] R. L. Weaver and J. Burkhardt, Chaos, Solitons Fractals **11**, 1611 (2000).
[9] P. Sebbah, D. Sornette, and C. Vanneste, Phys. Rev. B **48**, 12 506 (1993).
[10] A. MacKinnon and B. Kramer, Z. Phys. B: Condens. Matter **53**, 1 (1983).
[11] T. Ohtsuki, K. Slevin, and T. Kawarabayashi, Ann. Phys. (Leipzig) **8**, 655 (1999).
[12] N. Garsia and A. Z. Genack, Phys. Rev. Lett. **66**, 1850 (1991).
[13] S. K. Cheung, X. Zhang, Z. Q. Zhang, A. A. Chabanov, and A. Z. Genack, Phys. Rev. Lett. **92**, 173902 (2004).
[14] S. E. Skipetrov and B. A. van Tiggelen, Phys. Rev. Lett. **92**, 113901 (2004)
[15] D. Vollhardt and P. Wolfle, in *Electronic Phase Transitions*, edited by W. Hanke and Yu. V. Kopaev (Elsevier, Amsterdam, 1992).
[16] A. P. Prudnikov, Yu. I. Brychkov, and O. I. Marychev, *Integrals and Series* (Science, Moscow, 1981).